Chemical Engineering Journal 522 (2025) 166971

Contents lists available at ScienceDirect

Chemical Engineering Journal

journal homepage: www.elsevier.com/locate/cej

Unveiling the mechanism of ozone activation in water via singlet oxygen over cyclodextrin derived graphitic carbocatalysts

Antón López-Francés [a], Ana García-Mulero [b], Emanuela Accardo [b], Belén Ferrer [a], Antonio Franconetti [c], Ana Primo [b], Amarajothi Dhakshinamoorthy [a,d,*], Sergio Navalón [a,**], Hermenegildo García [b,**]

[a] Departamento de Química, Universitat Politècnica de València, Camino de Vera s/n, Valencia 46022, Spain
[b] Instituto Universitario de Tecnología Química (ITQ), Universitat Politècnica de València-Consejo Superior de Investigaciones Científicas (CSIC-UPV), Avenida de los Naranjos s/n, 46022, Valencia, Spain
[c] Departament de Química, Universitat Autònoma de Barcelona, 08193 Cerdanyola del Vallès, Spain
[d] School of Chemistry, Madurai Kamaraj University, Madurai 625 021, Tamil Nadu, India

ARTICLE INFO

Keywords:
Catalytic ozonation
Cyclodextrin derived graphitic carbocatalysts
Heterogeneous catalysis
Oxalic acid degradation
Singlet oxygen

ABSTRACT

Metal-free heterogeneous ozonation catalysis is recognized as a promising technology for water decontamination. Herein, we report the development of cyclodextrin (CD) derived graphitic (G) carbons through pyrolysis of α-, β- and γ-CDs under Ar atmosphere with fine-tuned activity as ozonation carbocatalysts for the degradation of oxalic acid in water. The G carbon obtained from α-CD showed the highest activity compared to its analogous solids under similar conditions. This solid was reused several times with a slight decrease in its activity, but after deactivation the performance of the fresh material can be restored in a large extent by a thermal pyrolysis treatment. Selective quenching experiments and electron spin resonance measurements with trapping agents revealed that O_3 is transformed by interaction with G into $^1O_2$ that becomes the active species. Experimental and computational evidence indicated that $^1O_2$ reacts with the graphitic domains of Gs via endoperoxide intermediate that is the responsible species for oxalic acid degradation. These novel findings underscore the unforeseen importance of carbocatalytic O_3 transformation into $^1O_2$ species that further react with graphitic domains of the carbocatalyst leading to the formation of endoperoxide intermediate that is a bis oxyl radical precursor responsible for oxalic acid degradation.

1. Introduction

Over the years, heterogeneous catalytic advanced oxidation processes (AOPs) based on transition metals have been one of the preferred technologies for water decontamination. [1–4] One of the main aims of these processes is the generation of reactive oxygen species (ROS) such as HO• or HOO• radicals from oxidants such as ozone (O_3), [5–8] H_2O_2, [9] peroxymonosulfate, [3,10] and persulfate [3,11,12] among others, which are able to degrade or mineralize many organic contaminants. Among them, catalytic ozonation is considered as a cost-efficient technology for pollutant degradation in water with potential implementation at large scale. [5,13] In fact, O_3 has been widely employed as oxidant or disinfectant in many large-scale drinking water treatment plants. [14] However, O_3 alone is incapable of degrading/mineralizing electron-poor organic pollutants that are, however, degraded and mineralized in larger extent by catalytic ozonation processes. [5,6] Regardless of the important achievements made in the field of catalytic AOPs using O_3 or other oxidants, some crucial aspects have limited their application. For example, some of the most active AOP catalysts or co-catalysts are based on critical and/or toxic transition metals such as cobalt. [7] Furthermore, long-term usage of metal-based heterogeneous catalysis under real conditions results in the occurrence of metal leaching from the solid catalyst to the aqueous media. Importantly, several studies have shown the possibility to replace transition metal-based advanced oxidation catalysts by carbon-based materials while achieving similar or even higher activities. [8,15–19] The list of carbonaceous materials includes activated carbon (AC), [9] graphite [20] or graphene-based materials, [21,22] carbon nanotubes, [23] and

* Correspondence to: A. Dhakshinamoorthy, School of Chemistry, Madurai Kamaraj University, Madurai 625 021, Tamil Nadu, India.
** Corresponding authors.
E-mail addresses: dhaam@itq.upv.es (A. Dhakshinamoorthy), sernaol@doctor.upv.es (S. Navalón), hgarcia@itq.upv.es (H. García).

https://doi.org/10.1016/j.cej.2025.166971
Received 11 April 2025; Received in revised form 25 July 2025; Accepted 7 August 2025
Available online 8 August 2025

nanodiamonds [24] among others. [15,19,25] It should be noted that the development of carbon-based materials derived from biomass resources as metal-free advanced oxidation catalysts for environmental remediation is a clear paradigm of sustainability. [26] For this purpose, biomass precursors like wood, pine needles, coconut shell, algae as well as monosaccharide like glucose or polysaccharide like starch have been employed. [27,28] Other studies have also shown development of graphitic carbon-based materials from cyclodextrins (CDs), cyclic oligomers of glucopyranose obtained from enzymatic transformations of starch, with unique morphological and physico-chemical properties that can determine their catalytic properties. [29] Interestingly, pyrolysis of α-, β- and γ-CDs that contain six, seven and eight glucose monomers results in the formation of nanoporous graphitic carbons with regular channel sizes having the dimensions of 0.38, 0.54 and 0.67 nm, respectively. In one of the related examples, α-CD derived graphitic carbon exhibited the highest catalytic activity among the series of samples tested for the molecular O_2 activation to oxidize benzylic alcohol. [29] It was proposed that the unique activity of graphitic carbon derived from α-CD is due to the tight fit of O_2 within its channels that favors the thermocatalytic electron transfer from the graphitic carbon to O_2 leading to the formation of $O_2^{\cdot-}$ radical species. In contrast, the lower catalytic activity of the graphitic carbon derived from β-CD or γ-CD is due to the gradual decrease of O_2 constrain with the graphitic carbon walls that make the formation of $O_2^{\cdot-}$ radicals.

In the field of metal-free carbocatalytic ozonation for aqueous pollutant degradation, most of the studies have proposed that O_3 is catalytically transformed into $HO^{\bullet}$ or $HOO^{\bullet}$ radicals that promote the degradation of contaminants via electron transfer processes. [19] Apart from these radical-based oxidations, some studies have reported that O_3 can be transformed into $^1O_2$. [19] It is a relatively mild oxidant ($E^0(^1O_2/O_2^{\cdot-}) = 0.81$ V) compared to $HO^{\bullet}$ ($E^0 = 2.81$ V) or $HOO^{\bullet}$ ($E^0 = 1.86$ V) radicals. The implementation of $^1O_2$ for practical applications in water decontamination is somehow limited to electron rich molecules via cycloaddition reactions to unsaturated organic compounds, activation of the allylic position or electron abstraction from electron-rich molecules. For these reasons, $^1O_2$ is not commonly considered as ROS responsible for the total organic carbon mineralization in water. [19] Interestingly, carbon-based materials such as AC, [30] graphites, [31–33] graphenes [34,35] or sp^2/sp^3 nanodiamonds [36] or some biomass-derived carbons such as alginate [37] have been reported for the transformation of O_3 into $^1O_2$. As commented earlier, $^1O_2$ is unable to degrade organic contaminants like oxalic acid in water under practical conditions for water treatment. In contrast, oxalic acid can be mineralized during the carbocatalytic ozonation process. It is assumed that $^1O_2$ should interact with carbon-based materials to form an intermediate, which is capable of degrading oxalic acid but, however, the nature of this intermediate is still to be revealed. Besides, the possibility of developing metal-free microporous graphitic carbons with regular pore sizes like those derived from CDs that can influence O_3 activation towards ROS has not yet been addressed.

With these precedents in mind, we report herein the development of metal-free graphitic (G) carbon derived from α-, β- or γ-CDs as ozonation catalysts for oxalic acid degradation in water. One of the innovations of this study is to investigate the importance of pore size diameter of the different G materials on their activity for O_3 activation towards the formation of ROS. The high reactivity of α-G derived from α-CD is due to its ability to react with O_3 to generate catalytically active $^1O_2$ which later interacts with α-G to promote oxalic acid mineralization. Experimental and computational evidence indicate the nature of the active sites on α-G and to support the role of $^1O_2$ to form endoperoxide intermediates on the carbon materials that promote catalytic reactions. This is the first study reporting the use of cyclodextrin-derived graphitic carbon for promoting $^1O_2$-mediated ozonation in water for oxalic acid degradation. The main novelty of our study, respect to the existing precedents is to provide evidence showing that $^1O_2$ generated from O_3 attacks the graphitic carbon forming endoperoxide-like intermediates that upon subsequent transformation can decompose oxalic acid. In that way, no direct contact between O_3 and oxalic acid is necessary.

2. Experimental section

The complete list of materials, reagents and solvents (Section 1.1) employed in this work are given in the supporting information (SI) file. In addition, a detailed procedure for the preparation of graphitic carbons like α-G, β-G or γ-G from the precursors of α-CD, β-CD and γ-CD, respectively is provided in the SI file (Section 1.2). On the other hand, derivatization of α-G, β-G or γ-G procedure (Section 1.3) is also given in the SI file. A catalytic procedure for the ozonation reaction for the decomposition of oxalic acid in water is discussed in detail in Section 1.4. Furthermore, Section 1.5 narrates the procedure for the regeneration of the partially deactivated α-G, β-G or γ-G solids. A list of characterization methods used in this work is provided in Section 1.6. In addition, the procedure followed to measure electron paramagnetic resonance (EPR) spectra with spin traps is described in Section 1.7. Photochemical $^1O_2$ generation in the presence of α-G, β-G or γ-G solids is given in Section 1.8. Details of the theoretical calculations are provided in Section 1.9.

3. Results and discussion

3.1. G preparation and characterization

α-, β- and γ-G samples were obtained from the commercially available α-, β- or γ-CDs as precursors, respectively by template-free pyrolysis under Ar atmosphere at 900 °C. The proposed pyrolysis mechanism leading from molecular CDs to the final microporous graphitic carbons goes through the melting of the solid CDs about 300–400 °C and assembly of the molecules with truncated cone shape in such a way that the smaller opening of one molecule assembles with the larger opening of the next one forming tubes that finally transforms at higher temperature into graphitic carbon by losing oxygen atoms almost completely. Considering that pyrolysis temperature is much higher than the melting point of the corresponding CD, the actual melting point value is not relevant, while the diameter of the final micropores is inherited from the dimensions of the CD precursor. Combustion elemental analyses revealed that carbon is the main element in α-, β- and γ-G solids with the values of 91, 90 and 87 %, respectively (Table S1). The presence of small percentage of nitrogen (< 0.23 wt%) is likely due to imperfect purification of CD after their enzymatic preparation [29]. In addition to the small fraction of hydrogen in all samples (0.5 wt%), the difference between 100 and the sum of the C, N and H percentages is assigned to oxygen. In addition, sample characterization by X-ray photoelectron spectroscopy (XPS) analyses showed the presence of C 1 s (Fig. 1b) and O 1 s (Fig. 1c). Additional details of XPS characterization for α-G, β-G and γ-G samples are shown in Figs. S1-S3 and Table S1). XPS region of C 1 s shows after deconvolution the presence of C═C sp^2 (284.4 eV), C—O (285 eV), C═O (288 eV), COO (290) and π-π* transition of carbon in aromatic moieties (291.5 eV) (Panel b in Figs. S1-S3 and Table S1). [38] XPS data of O 1 s can be fitted to the presence of C═O (530 eV), -OH/-O- (532 eV) and COO (534 eV) (Fig. 1 a-b, panel c in Figs. S1-S3 and Table S1). [38] XPS data of O 1 s can be fitted to the presence of C═O (530 eV), -OH/-O- (532 eV) and COO (534 eV) (Fig. 1 a-b, panel c in Figs. S1-S3 and Table S1). [38] Raman spectra of the Gs show the presence of two main bands at about 1350 and 1514 cm^{-1} characteristic of defective Gs and graphitic carbons, respectively (Fig. 1c, Fig. S4). [22] Specifically, in a carbon material the G band (1514 cm^{-1}) refers to ideal graphitic domains while the D band (1350 cm^{-1}) is related to the presence of structural defects like oxygen or nitrogen functional groups and carbon vacancies among other possibles. [19] In addition, the degree of graphitization of Gs can be determined by the I_D/I_G ratio from Raman spectra, the lower this ratio, the higher the graphitization degree. To put into context this I_D/I_G ratio, previous studies have reported

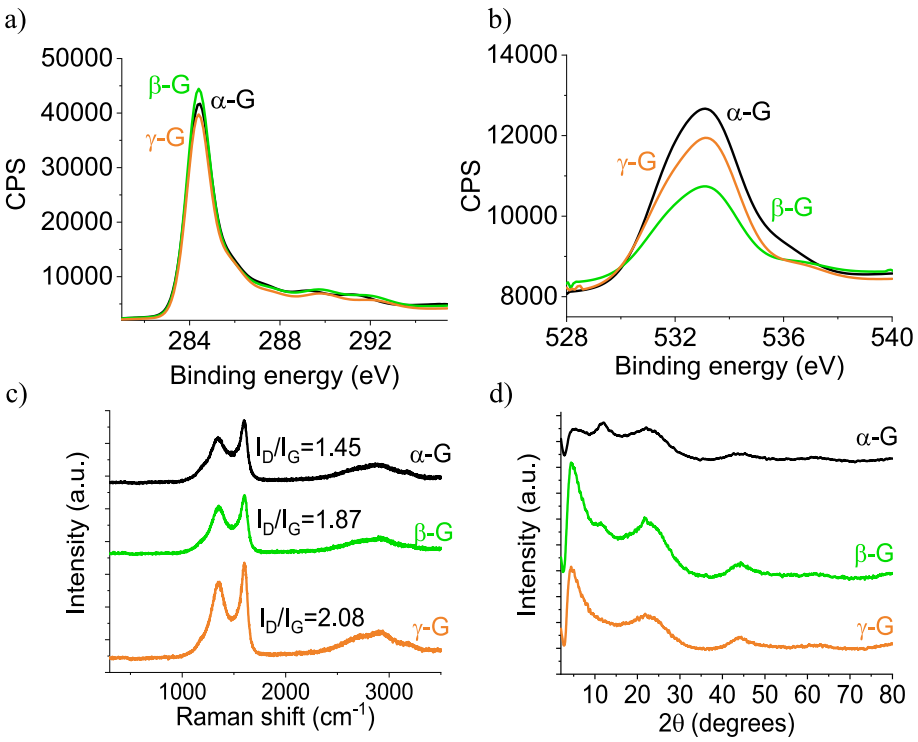

Fig. 1. a) XPS of C 1 s of α-G, β-G, γ-G, b) XPS of O 1 s of α-G, β-G, γ-G, c) Raman spectra of α-G, β-G, γ-G and d) powder XRD of α-G, β-G and γ-G solids.

for synthetic nanographite and oxidized nanographite with HNO_3 values of 0.55 and 1.19, respectively. [32] In the present case, the graphitization degree follows the order: α-G > β-G > γ-G, in where the estimated number of defects present in β -G and γ-G is about 30- and 140-times higher respect to α-G.

Powder X-ray Diffraction (XRD) of G solids are characterized by the presence of broad bands at about 25 and 42° associated with the graphitic domains (Fig. 1d). In addition to these bands, the presence of low angle bands associated to the regular channel porosity derived from the self-assembly of tronco-conical CD units forming tubes. [29] HR-SEM analyses show the presence of graphitic layers (Fig. 2). Further, HR-TEM analyses of the α-, β- and γ-G samples indicate the presence of channels with diameter dimensions of 0.625, 0.798 and 1.066 nm, respectively (Figs. 2 and S5). It should be noted that these CD diameters correlate with the sizes of α-, β- and γ-CD precursors formed by cyclo-oligomerization of 6, 7 and 8 glucopyranose units with dimensions of about 0.5, 0.6 and 0.8 nm, respectively [39,40]. Additional HR-TEM measurements at higher magnification allowed to determine interlayer distances of about 0.35 nm characteristic of graphitic carbon layers in a turbostratic carbon. Thus, it is proposed that during the heating process under Ar atmosphere, upon melting about 300 °C, molten CDs undergo supramolecular arrangements forming tubes that subsequently undergo graphitization at higher temperatures, rendering graphitic carbons with microporous channels of similar dimensions to those of the CD precursors. [29] Isothermal N_2 sorption measurements (Fig. S6) show a BET surface area of 482, 417 and 251 $m^2\ g^{-1}$ for α-G, β-G and γ-G solids, respectively. The isothermal gas sorption data corresponds to Type I type plots that also reveal the presence of microporous channels in the Gs.

3.2. Catalytic ozonation

Oxalic acid is a common probe molecule that has been often used to determine the relative activity of solid catalysts for ozonation. [19,32] Thus, the performance of α-, β- and γ-G as ozonation solid catalysts was investigated in the degradation of oxalic acid. The results obtained are presented in Fig. 3a. As can be seen, oxalic acid degradation does not occur in the absence of Gs, the adsorption of oxalic acid is <2 % using different Gs. In sharp contrast, the α-, β- and γ-G materials promote oxalic acid degradation, but the catalytic activity of these samples depends on the nature of precursor. Thus, the most active solid is α-G derived from α-CD. It is important to note that previous studies have proposed that the active sites are electron-rich sp^2 carbon domains in graphitic carbon-based materials such as graphites, ACs or carbon nanotubes [18,19]. In this work, the degree of graphitization based on both the sp^2 fraction determined by XPS and I_D/I_G ratio measured by Raman spectroscopy follows the order of α-G > β-G > γ-G. Furthermore, accessibility to the active sites is commonly related to the porosity of the samples, the higher the surface area and pore volume, the higher the accessibility of reagents to the active sites is [19]. From these grounds, it is likely to propose that the order of catalytic activity of Gs can be associated with the graphitization degree that is related to the presence of active sites and their porosity allowing reagent diffusion. In this way, the G sample with the highest graphitic character and surface area being the one with the highest activity, namely α-G. Besides, as will be shown later, mechanistic studies involving experimental and theoretical calculations indicate that the higher curvature of graphitic walls favors its reactivity with catalytic generation of $^1O_2$ from O_3 via endoperoxide intermediate formation and subsequent generation of bis oxyl radicals which are responsible for oxalic acid degradation. These findings agree with the observed order of reactivity and wall diameter of Gs for oxalic acid degradation, i.e. α-G with the smallest wall diameter exhibits the highest activity.

The influence of the initial pH in the reaction medium was studied for the degradation of oxalic acid with O_3 as an oxidant by screening the pH values from 3 to 11 (Fig. 3b). It was observed that although the influence was relatively minor at initial neutral or acid pH values, acid pH values increase the decomposition rate to some extent from pH 7 to 3, while a complete degradation of oxalic acid was achieved at pH 3. In these cases, initial pH values from 3, 5 and 7 decreased at the end of the reaction to 2.6, 4.5 and 6.3, respectively. In contrast, oxalic acid decomposition is disfavored by initial basic pH values, the slowest

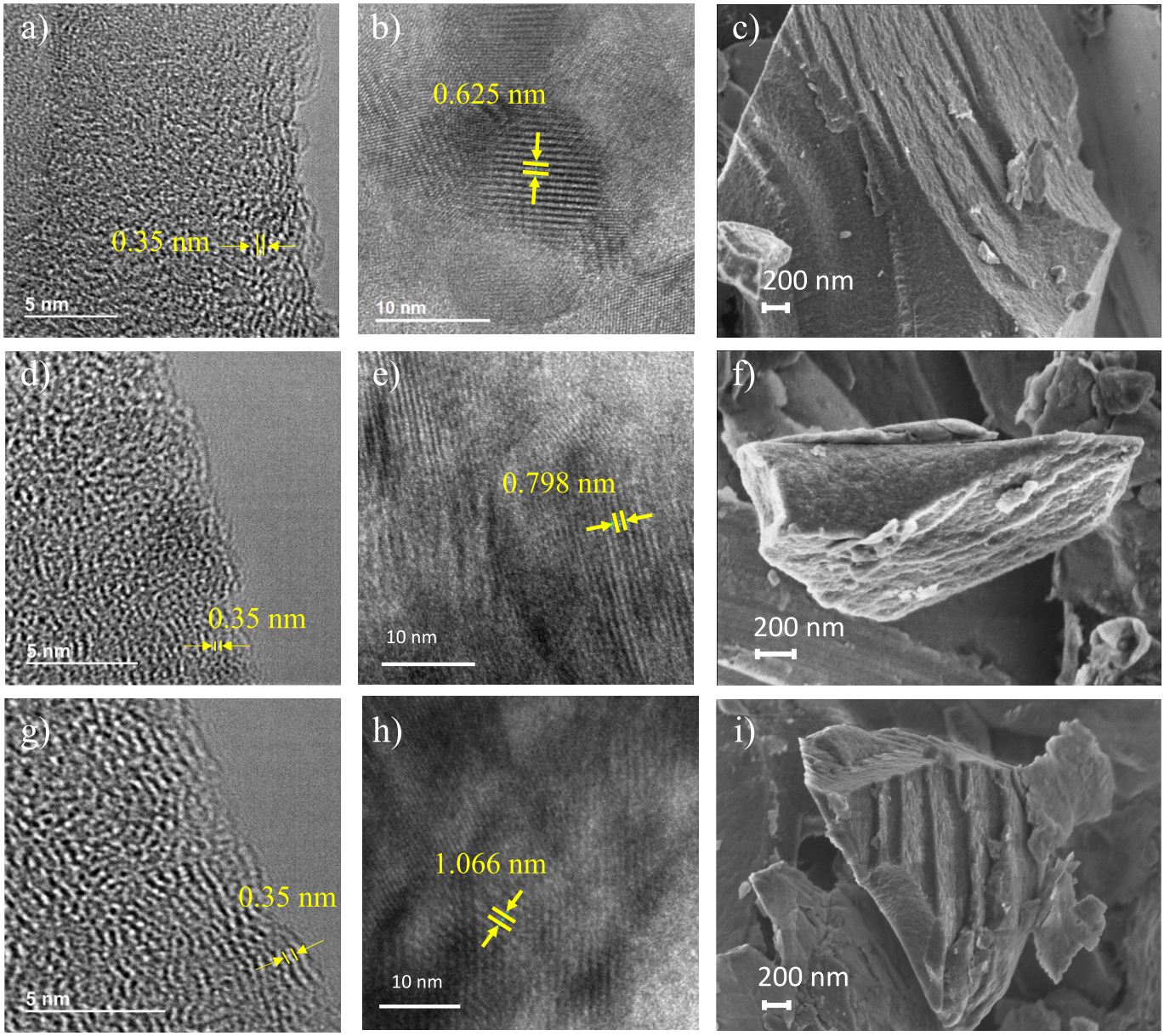

Fig. 2. HR-TEM images of α-G (a, b), β-G (d, e), γ-G (g, h) and HR-SEM images of α-G (c), β-G (f) and γ-G (i) solids.

decomposition rate being measured at pH 11. Therefore, it is reasonable to propose that the highest activity observed at acidic pH values can be correlated with the higher concentration of O_3 available in water that can be catalytically transformed into ROS (see Section 3.3) that are presumed to be the species that decomposes oxalic acid in water. To evaluate potential differences in reaction rates for oxalic acid degradation as a function of the initial pH, the initial reaction rate (r_0) was estimated from oxalic acid degradation data shown in Fig. 3a. In the case of catalytic experiments carried out at initial pH 9 and 11 the temporal profiles showed an induction period up to 60 min. For these tests, the r_0 values were estimated at 60 min. The r_0 for oxalic acid degradation at pH 3, 5, 7, 9 and 11 were 0.026 mg L^{-1} min^{-1}, 0.015 mg L^{-1} min^{-1}, 0.006 mg L^{-1} min^{-1}, 0.0054 mg L^{-1} min^{-1} and 0.0033 mg L^{-1} min^{-1} respectively. After correction for the induction period, the results indicate a linear decrease of the r_0 as the pH increases. It should be noted that the order of catalytic activity as a function of pH agrees with the order of O_3 stability in water, [5,31] the highest activity achieved at acidic pH values corresponding to the range of maximum O_3 stability in water and vice versa. In our study, stationary O_3 concentration in water upon its continuous supply (140 mg h^{-1}) to the ozonation system at pH values of 3, 5, 7, 9 and 11 was 12.48, 10.56, 8.16, 4.32 and 1.44 mg L^{-1}, respectively. Therefore, it is proposed that the highest activity observed at acidic pH values can be correlated with the higher concentration of O_3 available in water that can be catalytically transformed into ROS (see Section 3.3) that are presumed to be the species that decompose oxalic acid in water. In addition to these comments, it is important to highlight that α-G exhibits relatively broad range of activity as a function of the pH compared to previous analogous reports using AC, [30] graphitic carbons [37] or hybrid sp^2/sp^3 nanohybrids [36] with activities restricted to pH values below 5. The relatively good performance of α-G in a broad range of pH could be attributed to the effect of porosity that adsorbs O_3 within the channels in a close proximity to the active sites to produce ROS, as it will be discussed in latter sections describing the results of EPR, selective quenching experiments and computational results.

Heterogeneity and catalyst stability are two most important issues in heterogeneous catalysis. The fact that the reaction occurs due to the solid catalyst and not due to any possible species that become dissolved in the solution was confirmed by performing an analogous experiment

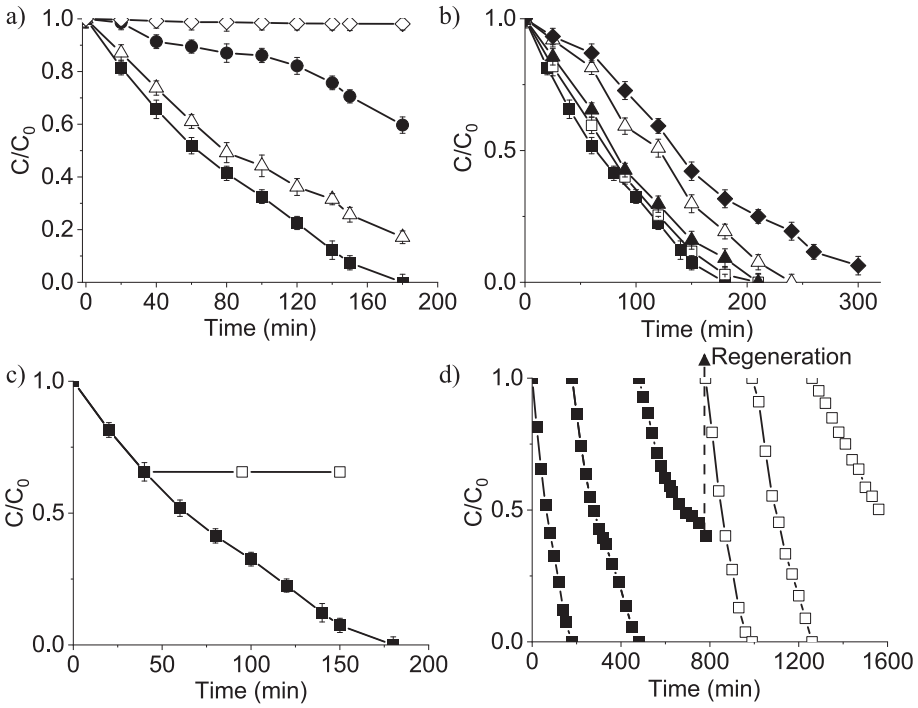

Fig. 3. a) Metal-free catalytic ozonation of oxalic acid in water at pH 3. Legend: O_3 (◆), α-G (■), β-G (▲) and γ-G (●); b) Carbocatalytic ozonation of oxalic acid at different initial pH values at pH 3 (■), pH 5 (□), pH 7 (▲), pH 9 (△), pH 11(◆) using α-G; c) Hot-filtration test with α-G (■) and upon removal of α-G after 25 min (□) and d) reusability and regeneration of α-G. Reaction conditions: Oxalic acid (50 mg L^{-1}), carbocatalyst (100 mg L^{-1}), temperature 20 °C, O_3 inlet to the glass reactor (140 mg h^{-1}).

under typical reaction conditions in which the solid was filtered once a certain conversion has been achieved. After removal of the solid, the reaction was allowed to continue in its absence. In the present case, Fig. 3c shows that the solid is filtered at about 35 % oxalic acid conversion and the solution without catalyst shows no further degradation. This confirms that the reaction is taking place exclusively by the presence of α-G as the solid catalyst, providing firm evidence for the heterogeneity of the process.

To assess the catalyst stability, a series of consecutive reuses were performed using α-G as a catalyst. The results are presented in Fig. 3d. A certain deactivation was observed from the first to the second run, that was particularly evident by the longer reaction required for complete degradation of oxalic acid. This deactivation of α-G was more clearly evidenced in the 3rd use, for which only 50 % of oxalic acid disappearance was achieved at final reaction time compared to the first use. Considering that the catalyst was used in three consecutive runs,

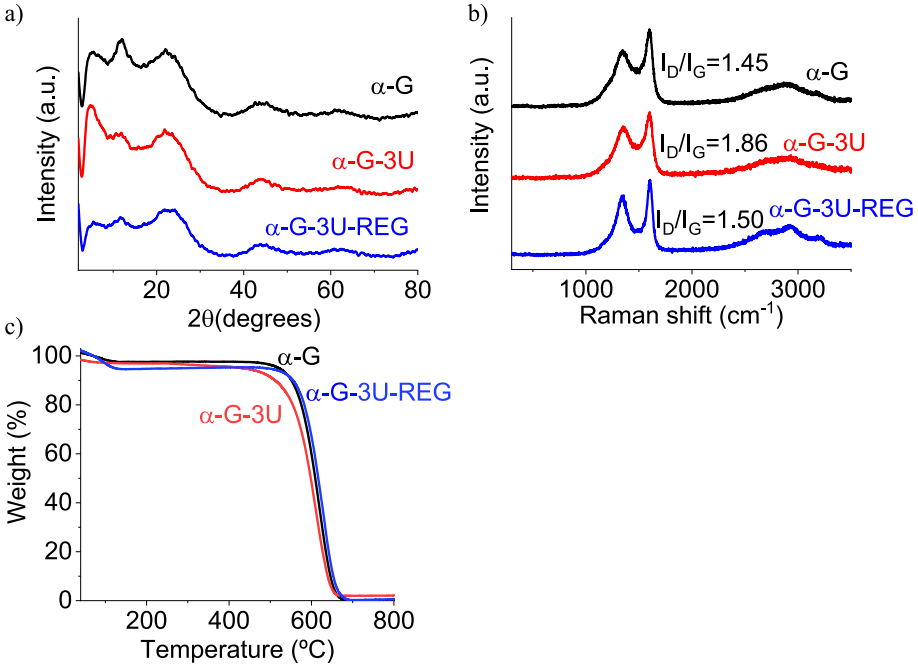

Fig. 4. a) Powder XRD of α-G, α-G-3U, α-G-3U-REG, b) Raman spectra of α-G, α-G-3U, α-G-3U-REG and c) TGA of α-G, α-G-3U and α-G-3U-REG.

decomposing oxalic acid (50 mg L^{-1}) in certain proportions according to the reuse employing α-G at 100 mg L^{-1}, the minimum specific activity of the material is 1.44 mM/$g_{α-G}$.

To understand the origin of partial deactivation of α-G sample upon reuses, the recovered solid after 3rd use (α-G-3U) was characterized and compared to the pristine α-G material. Although powder XRD showed minor changes (Fig. 4a), Raman spectroscopy (Figs. 4b, S7) revealed a relative increase in the density of defects in the graphitic structure by increasing I_D/I_G value from 1.45 to 1.85 for the fresh α-G and α -G-3U sample, respectively. [22] Also, XPS data show a decrease in the proportion of graphitic sp^2 C from 60 to 34 % for the α-G and α-G-3U accompanied by an increase of oxygen-functional groups such as alcohol, ketone and carboxylates in O 1 s XPS region, again indicating that the O_3 treatment partially oxidizes the graphitic material (Figs. S8 and S9 and Table S2). In fact, HR-TEM analyses of α-G-3U allowed determining the presence of interplanar distances of about 0.385 and 0.219 nm characteristic of sp^2 C—C in graphitic domains accompanied by sp^3 C—C, respectively. Furthermore, α-G-3U showed lower thermal stability than pristine α-G associated with a higher population of unstable oxygen-functional groups of the former (Fig. S10 and S11). The information from the series of characterization techniques suggests that these defects could be related to the introduction of oxygenated groups on the graphitic structure of α-G-3U. If this hypothesis is valid, pyrolysis of α-G-3U under Ar at high temperatures (i.e. 900 °C) could decompose oxygen functional groups into CO_2, CO and H_2O producing some degree of regraphitization [32,41]. Hence, α-G-3U sample was submitted to pyrolysis treatment with the aim to remove these oxygen atoms (α-G-3U-REG). Interestingly, α-G-3U-REG has recovered the initial graphitization degree as of α-G to a larger extent as evidenced by Raman spectra (Fig. 4b and Fig. S7), XPS (Figs. S8, S9 and Table S2), thermogravimetric analysis (TGA) (Fig. 4c) and HR-TEM (Figs. S10 and S11) techniques. Furthermore, α-G-3U-REG exhibited an identical temporal profile for oxalic acid degradation as that of the fresh α-G, indicating that the deactivated sample can be regenerated by removing oxygenated functional groups. Regardless of these comments, for practical applications it would be convenient to regenerate the carbocatalyst under milder conditions. In this context, previous studies have reported the possibility of biomass carbonization using hydrothermal carbonization processes that commonly operate at temperatures ranging from 180 to 240 °C and these methodologies might be also suitable for α-G-3U regeneration. [42]

Additionally, a productivity test (Fig. S12) in where large amounts of oxalic acid (1 g L^{-1}) was used in the presence of α-G (100 mg L^{-1}) as a catalyst showing a full degradation of oxalic acid after 40 h. A similar experiment with the reduced loading of α-G (50 mg L^{-1}) also degraded oxalic acid after 80 h, meaning that α-G can perform more than 200 $mmol^{-1}_{oxalic\ molecules\ gcatalyst}$ turnovers.

The catalytic activity achieved using α-G was compared with previous analogous carbocatalysts for oxalic acid ozonation degradation in water (Table S3). Recently, an activated biochar derived from pine needle waste biomass as ozonation catalyst (50 mg L^{-1}) was able to degrade oxalic acid (1 g L^{-1}) at pH 3 and 140 mg h^{-1} O_3 in about 255 h [43], 3.2 more time than required using α-G. In other study, the use of a defective structured graphitic carbon synthesized from alginate as biomass source used as ozonation catalyst (50 mg L^{-1}) for oxalic acid degradation (1 g L^{-1}) at pH 3 and a O_3 flow 140 mg h^{-1}, required 2.8-fold more time than in the case of α-G. [37] In other study, a regenerated field-spent granular AC was able to degrade oxalic acid (1 g L^{-1}) under similar reaction conditions (pH 3, 140 mg h^{-1} O_3) in about 57 h but using four times larger catalyst amount (200 mg L^{-1}) than α-G. [30] These experiments indicate the superiority and long-term stability of α-G as a biomass-based carbocatalyst for the degradation of oxalic acid, an activity that according to the pH influence can be attributed to the effect of microporosity. Regardless of these comments, there is still much room for improvement of the carbocatalytic activity of biomass-derived materials to achieve activity of a non-biomass synthetic nanographite ozonation catalyst (50 mg L^{-1}) able to degrade oxalic acid (1 g L^{-1}) in water at pH 3 in about 11 h. [32]

3.3. Nature of ROS and active sites on α-G

3.3.1. ROS generation

Previous related studies have proposed that the ability of graphitic carbon-based materials for O_3 decomposition can be correlated with the generation of ROS and, therefore, with the order of catalytic activity during pollutant degradation. [44] Fig. S13 shows that Gs have a similar ability for O_3 decomposition, α-G being slightly more active followed by β-G and γ-G. Interestingly, this order is similar for the catalytic oxalic acid decomposition (Fig. 3a). As will be shown below, the order of O_3 decomposition by Gs correlates with the measured order of EPR spectra intensities with 2,2,6,6-tetramethylpiperidine (TEMP) and 5,5-dimethyl-1-pyrroline-N-oxide (DMPO) as spin traps.

To get information about the role of α-G as carbocatalyst and, particularly, how O_3 reacts with G, a control experiment was carried out. Specifically, α-G was exposed to O_3 for 1 h. Then, the ozonator was disconnected and only air was introduced in the system to guarantee carbocatalyst suspension in water. Immediately, oxalic acid dissolved in water (1 mL) was introduced to the reactor to achieve a concentration of 25 mg L^{-1}. In this way, if some active sites are created on the surface of the α-G acting as stoichiometric sites for oxalic acid degradation, a significant decrease in oxalic acid concentration should be observed. Previous studies have shown that removal of oxalic acid catalyzed by AC requires about 0.42 to 0.77 mol of O_3 per mol of oxalic acid degraded. [45] However, it should be noted that oxalic acid degradation does not occur in the presence of O_3 and absence of carbocatalyst under the studied reaction conditions (Fig. 3a). The temporal profile for the degradation of oxalic acid in the presence of previously ozonated α-G and in the absence of additional O_3 supply is shown in Fig. 5a. The temporal profile for the degradation of oxalic acid is shown in Fig. 5a. As can be seen, the oxalic acid concentration decreases by half after 40 min and then remains constant from 40 to 100 min. This behavior suggests the generation of a certain population of active sites on the surface of α-G upon O_3 treatment for 1 h that subsequently can promote oxalic degradation. In other words, the sites generated in α-G by reaction with O_3 can promote oxalic acid degradation on their own without the need for additional O_3. Once the active sites on the α-G surface are depleted, no further oxalic acid degradation occurs. This observation is compatible with an increase in the population of oxygen functional groups, such as carbonyl, alcohol and ether, observed in the α-G-3U sample as previously commented (Fig. S8 and Table S2). It should be commented that the possibility that O_3 becomes adsorbed on α-G without reacting with its graphitic structure, although less likely due to the low O_3 concentration in water and the O_3 tendency to decompose, cannot be rigorously ruled out. Furthermore, additional support to surface modification of α-G by O_3 was obtained by Raman spectroscopy. Fig. 5b shows that the Raman analysis of O_3-treated α-G exhibits an increase in the I_D/I_G ratio (2.12) compared to the fresh sample (I_D/I_G = 1.45; Fig. 1a), indicating the generation of structural defects in the O_3-treated α-G.

After having confirmed that oxalic acid degradation is caused by some oxygenated species formed on the surface of α-G, it was of interest to determine whether O_3 was the only ROS responsible for the activation of α-G or whether α-G was also undergoing transformation by other O_3 derived species. For this purpose, initially a series of catalytic quenching experiments using inorganic anions were performed. It was observed that inorganic ions such as HCO_3^-, [46,47] or $H_2PO_4^-$, [48] which are typical quenchers of HO• radicals, [46–48] did not interfere with the catalytic O_3 degradation of oxalic acid at pH 7 by α-G (Fig. S14a). Similarly, the presence of Cl^- anions do not inhibit catalytic oxalic acid degradation at pH 3 and 7 [47], thus providing another indirect probe of the absence of HO• radicals in our system (Fig. S14a, b). This conclusion was also confirmed by the lack of influence of organic quenchers of HO• radicals like dimethyl sulfoxide (DMSO), methanol or *t*-butanol during

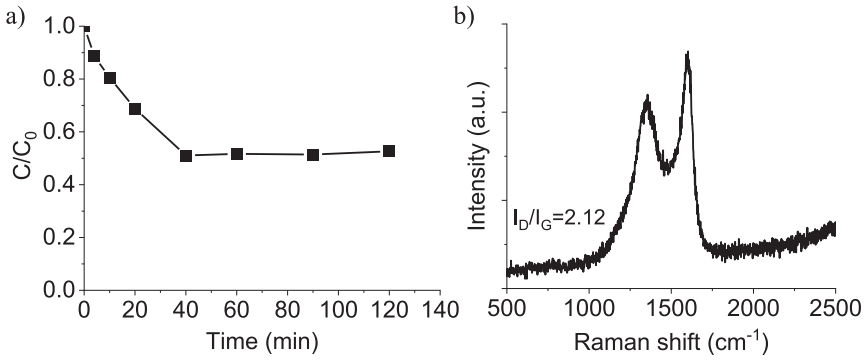

Fig. 5. a) Temporal profile of oxalic acid degradation by O_3-treated α-G for 1 h in water without additional supply of O_3; b) Raman spectra of O_3-treated α-G for 1 h. Reaction conditions: Oxalic acid (25 mg L^{-1}), α-G treated with O_3 (100 mg L^{-1}), pH 3, temperature 20 °C, O_3 inlet to the glass reactor (140 mg h^{-1}) only in the first step to react with α-G.

catalytic ozonation of oxalic acid (Fig. 6a). To get more evidence about the nature of ROS, the so-called quenching method was used. It is important to highlight that regardless of the widely used quenching method for years to verify the presence of ROS, some relative recent studies have raised concerns about the reliability of these methods. [8,49] It is proposed that the high concentration of quenchers employed results not only in quenching of target ROS but also can provoke changes in the reaction mechanism. Specifically, the validity of the quenching method assumes that the added quencher inhibits only the target ROS without affecting the reactions of O_3, other ROS and without altering the elemental steps of the reaction mechanism either in solution or surface-mediated. This assumption has been recently questioned, and it is under debate. In this work, the lack of influence of organic quenchers of HO• radicals, like DMSO, methanol or *t*-butanol. During catalytic ozonation of oxalic acid (Fig. 6a) seems also to indicate the absence of these radicals in our catalytic system. Regarding the role of *t*-butanol as HO• quencher, previous studies have reported that this molecule can trap these radicals in solution but not in carbon surface, therefore, it is not an appropriate quencher to rule out the possibility of hydroxyl-surface mediated reactions for pollutant degradation. [50–52] Similarly, no effect was observed with the presence of *p*-benzoquinone as $O_2^{\bullet-}$/HOO• quencher on the catalytic oxalic acid degradation by α-G, thus suggesting the involvement of these radicals in the process. A more reliable technique to identify the formation of ROS is EPR spectroscopy in the presence of spin traps. [8] In this study, EPR spectroscopy measurements using DMPO as spin trap only revealed the formation of $DMPO_X$ species with a characteristic five line spectrum having the hyperfine coupling constants of $A_N/G = 7.3$ and $A_H/G = 4.02$ (Fig. S15a,b). [53] Although $DMPO_X$ can be formed either by O_3 or several ROS such as HO•, $O_2^{\bullet-}$/HOO• or $^1O_2$, it should be noted that the observed intensity of $DMPO_X$ signal (Fig. S15a) for the three G materials agrees with the order of the observed catalytic activity α-G > β-G > γ-G (Fig. 3a). The use of N-*tert*-butyl-α-phenylnitrone (PBN) as spin trap did not show the formation of any radical adduct (Fig. S15c). In addition, selective quenching experiments with NaN_3 and furfuryl alcohol for $^1O_2$ showed a significant decrease of oxalic acid degradation (Fig. 6a), suggesting the formation of $^1O_2$ from O_3. The fact that neither NaN_3 nor furfuryl alcohol carbocatalytic oxalic acid decomposition in the presence of α-G.

Accordingly, it is proposed that O_3 and $^1O_2$ are the two active oxygen species involved during carbocatalytic oxalic acid decomposition in the presence of α-G. Previous studies have proposed that graphitic carbon with delocalized π electrons that can favor carbon surface-O_3 complexing structures can drive organic oxidation by intramolecular electron processes. [19] Other reports have proposed O_3 decomposition within electron rich sp^2 aromatic carbons leading to the formation of surface-adsorbed atomic oxygen with high oxidation potential (2.43 V) and capable to oxidize organic compounds. [19]

The involvement of $^1O_2$ in oxalic acid degradation was recently reported by some of us in the presence of carbon-based catalysts with graphitic domains [30,32,37] although the reasons behind the reaction pathway are still unclear. As it will be shown later, oxalic acid can be degraded in the presence of α-G and $^1O_2$ via endoperoxide intermediate with formation of oxidant oxyl radicals and surface-mediated oxalic degradation. Related with carbocatalytic ozonations for pollutant degradation via surface-mediated mechanisms, a recent study has reported a quantification of the contribution of heterogeneous surface

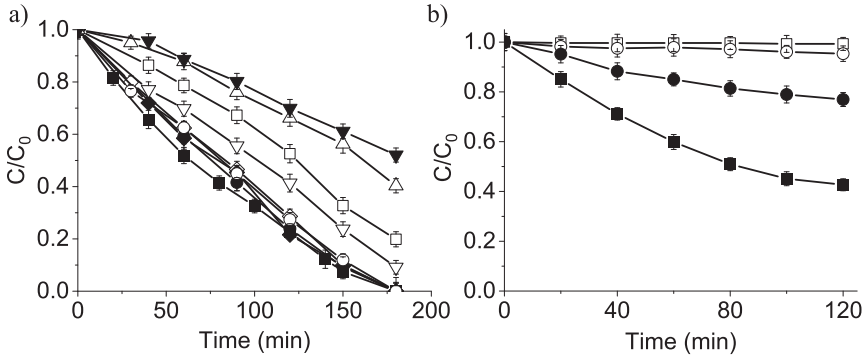

Fig. 6. (a) Carbocatalytic ozonation of oxalic acid at pH 3 using α-G as carbocatalyst in the absence (■) or in the presence of DMSO (●), *t*-butanol (▲), methanol (⋄), *p*-benzoquinone (○), NaN_3 (□) and furfuryl alcohol (△). Reaction conditions: Oxalic acid (50 mg L^{-1}), α-G (100 mg L^{-1}), temperature 20 °C, O_3 inlet to the glass reactor (140 mg h^{-1}). (b) Metal-free catalytic degradation of oxalic acid in water at pH 3 using α-G as carbocatalyst and Rose Bengal (50 mg L^{-1}). Legend: irradiating with absence of both Rose Bengal and catalyst (□), irradiating with Rose Bengal (○), irradiating for 30 min Rose Bengal and α-G without oxalic acid, after 30 min irradiation stops and oxalic acid is added (●), irradiating with Rose Bengal and α-G (■) and irradiating with Rose Bengal, α-G and adding furfuryl alcohol (△). Reaction conditions: Oxalic acid (20 mg L^{-1}), α-G (100 mg L^{-1}), temperature 20 °C.

processes to pollutant abatement during heterogeneous catalytic ozonation. [54] The characterized ROS involve O_3, $HO^{\bullet}$ and $O_2^{\bullet-}$. It was concluded that pollutants with low affinity for reduced graphene oxide surface were mainly degraded via bulk reactions and negligible contribution of heterogeneous surface-mediated degradation. For those cases that pollutants have good affinity for carbocatalyst surface, heterogeneous surface processes become important and even dominate their degradation. These results highlight the complexity of carbocatalytic ozonation of pollutants and the formation of various ROS with different oxidation capabilities that could be beneficial for pollutant degradation in real water matrices.

To provide additional experimental support for the generation of $^1O_2$ from O_3, EPR measurements using TEMP as a selective $^1O_2$ spin trapping agent were conducted with α-G as a catalyst. In agreement with the previous findings, the characteristic three equally intense peaks corresponding to TEMPO radical were observed. Fig. S15d,e shows the EPR spectrum of TEMPO recorded with the TEMP trapping experiment from O_3, compared with the simulated EPR spectrum of TEMPO with hyperfine coupling constant of $A_N/G = 17.3$ (Fig. S15e). [55] In summary, EPR and selective quenching experiments using NaN_3 and furfuryl alcohol confirm the catalytic generation of $^1O_2$ as ROS involved in oxalic acid degradation.

Oxalic acid degradation by catalytic ozonation is generally assumed as being specific of $HO^{\bullet}$ as a key reactive oxygen intermediate. [19] Accordingly, the role of the catalyst is typically assumed to be the generation of $HO^{\bullet}$ radicals, most commonly through electron transfer-proton coupled O_3 decomposition processes. This is not the case using α-G as a carbocatalyst. On one hand, the active oxygen center is anchored on the carbon surface. On the other hand, these oxygen sites are generated, at least in part through $^1O_2$. The present findings open therefore new views and possibilities on O_3 activation by a carbocatalyst. To obtain solid support for the role of O_3-derived $^1O_2$ in the degradation of oxalic acid, a series of experiments was carried out using typical $^1O_2$ generators as Rose Bengal photosensitizer. As can be seen in Fig. 6b, aerated Rose Bengal irradiation with simulated sunlight irradiation does not decompose of oxalic acid. When irradiation with visible light was performed using Rose Bengal as photosensitizer, degradation of oxalic acid degradation was observed after 2 h. In contrast, an irradiation with visible light in the presence of Rose Bengal as $^1O_2$ generator and α-G as catalyst resulted in a gradual decomposition of oxalic acid reaching 50 % after 2 h. Furthermore, if Rose Bengal and α-G are irradiated with visible light for 30 min in the absence of oxalic acid and then, oxalic acid is added while the system is kept in the dark, 20 % oxalic acid degradation was achieved. These experiments confirm that $^1O_2$ generated by irradiation of Rose Bengal can modify α-G, generating oxygenated surface groups that subsequently decompose oxalic acid.

3.3.2. *Selective masking of oxygen functional groups in α-G*

In order to gain information on the nature of the active sites in α-G that could be involved in the catalytic oxalic acid decomposition by α-G and considering that oxygenated groups present in carbonaceous materials have been proposed to be responsible for their catalytic activity in many cases, a series of control catalysts was prepared by selectively masking various possible oxygenated functional groups on α-G [56]. Scheme 1 illustrates the masked functional group, the reagent in the transformation and the simplified structure of the derivatized functional groups. Following the previous reports for the selective functional group masking in graphitic materials [57], phenylhydrazine, benzoyl chloride and phenacyl bromide were used to specifically mask C═O, C-OH and C-OOH groups, respectively, on α-G.

The derivatization of α-G was confirmed by XPS analyses (Figs. S16-S18 and Table S4). As expected, based on the prior literature data [57], XPS analysis confirmed the presence of nitrogen in α-G-CO, that appears as a single component peak in N 1 s with a binding energy of 400.6 eV. The masking of hydroxyl group in α-G with benzoyl chloride (α-G-COH) shows an increase of C 1 s components appearing at 288.4 and 288.65 eV corresponding to aromatic and carboxylic ester carbon, respectively. In addition, O 1 s XPS shows also an increase of carboxylic ester oxygen at 534 eV. Similarly, masking of the carboxylic acid groups by phenacyl bromide (α-G-COOH) increases the proportion of surface carbonyl oxygens at 534 eV and the corresponding carbon component at 288 eV, in accordance with the structure of the derivative. Overall, these XPS analyses support the functionalization of the corresponding oxygenated groups present in α-G.

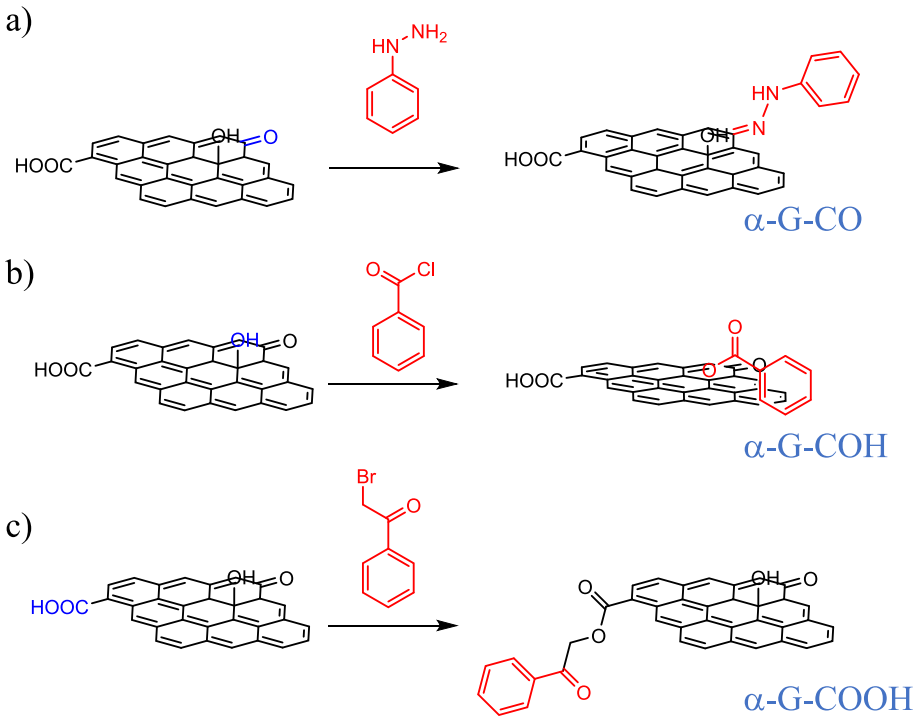

Scheme 1. Selective masking of oxygenated functional groups in α-G sample by selective derivatization of carbonyl, hydroxyl and carboxylic acid groups.

The temporal profile of oxalic acid degradation by O_3 of these three α-G derivatives is very similar to the kinetics of the α-G sample (Fig. S19). These results, therefore, unambitiously indicate that none of these oxygen functional groups are involved as active sites during the catalytic ozonation. Thus, it is proposed that it is the graphene C═C bonds the most likely active site in ozonation catalysis. This proposal is supported by the behavior of organic compounds as described in the sequel (Section 3.3.3). It should be noted that O_3 decomposition by functionalized α-G is practically similar as observed for pristine α-G, thus indicating that these derivatizations do not have a significant impact on O_3 consumption (Fig. S20).

3.3.3. Organocatalytic model compounds

Based on the previous results as well as the chemical knowledge on the reactivity of $^1O_2$ with heterocycles and polycyclic aromatic compounds [58,59], we wanted to explore the catalytic activity of organic molecules that could have the same or similar structure as the ozonation active sites on α-G. Thus, a series of water-soluble organic molecules were selected, including tetrahydrofuran, furan and two anthracene derivatives namely 3,3′-(anthracene-9,10-diyl)dipropanoic acid and 2-aminoanthracene. While tetrahydrofuran practically does not promote organocatalytic oxalic acid ozonation (Fig. 7a), the other three organic molecules tested exhibit an obvious catalytic activity for oxalic acid decomposition. As shown in Fig. 7b, oxalic acid decomposition increased as the concentration of furan increased under the same conditions, i.e. an increase in the number of molecules present corresponds to a linear increase in the number of active sites, as can be seen in Fig. S21a. Similarly, the degree of oxalic acid degradation was increased as the concentration of 3,3′-(anthracene-9,10-diyl)dipropanoic acid increased in the presence of O_3 (Fig. 7c) (Fig. S21b). Although the water solubility of 2-aminoanthracene was limited to about 10 mM, oxalic acid degradation by O_3 also occurred with this compound (Fig. 7d) with an initial rate dependent on the concentration of 2-aminoanthracene (Fig. S21c).

Furthermore, an experiment in which 3,3′-(anthracene-9,10-diyl) dipropanoic acid was first treated with O_3 for 30 min in the absence of oxalic acid and then oxalic acid was added after 5 min results in 9 % oxalic acid degradation, indicating that the endoperoxide groups formed (see below) in the anthracene moiety are responsible for promoting oxalic acid degradation. The reaction of 3,3′-(anthracene-9,10-diyl) dipropanoic acid with O_3 was followed by UV–vis absorption spectroscopy. The disappearance of the characteristic absorption bands corresponding to the anthracene ring from about 350 to 425 nm was observed in UV–vis spectroscopy, indicating the formation of the oxygenated derivative disrupting the aromatic conjugation (Fig. S22) in good agreement with previous analogous reports. [60]

Therefore, based on the previous study on the role of $^1O_2$, the known reactivity of $^1O_2$ of furan, anthracene derivatives and the spectroscopic data obtained, a plausible reaction pathway for oxyl radical formation by O_3 in the case of anthracene-based organocatalyst is proposed in Scheme 2. As can be seen in this proposal, the first reaction occurs between $O_3/^1O_2$ with the organocatalyst resulting in the formation of stable endoperoxide which decomposes forming oxyl radicals. These oxyl radicals in water should be the active species responsible for the decomposition of oxalic acid. An analogous mechanism, but involving aromatic domains in G with formation of endoperoxides and peroxyl radicals, could also take place in G and cause oxalic acid decomposition.

This proposal is compatible with the observed increase in oxygen content of G during ozonation and the gradual deactivation of the material with increasing oxygen content, probably by depletion of the structural aromatic domains that react with $^1O_2$. Thermal treatment to remove H_2O, CO and CO_2 and rearomatization should restore catalytic activity.

3.3.4. Endoperoxide intermediate characterization on α-G

To gain evidence about endoperoxide on carbocatalyst surface, α-G was ozonated in water over time and sample suspensions analyzed by Raman and ATR FT-IR spectroscopies. Previous studies have reported that organic peroxide characterization by FT-IR spectroscopy results in week bands due to O—O stretching vibration which are relatively more intense in the case of Raman spectroscopy ranging from about 650 to 950 cm^{-1} depending on the type of peroxide. [61,62] Regardless of these comments, ATR FT-IR spectra (Fig. S23a,b) of ozonated α-G samples in water do not reveal the presence of new bands that could be

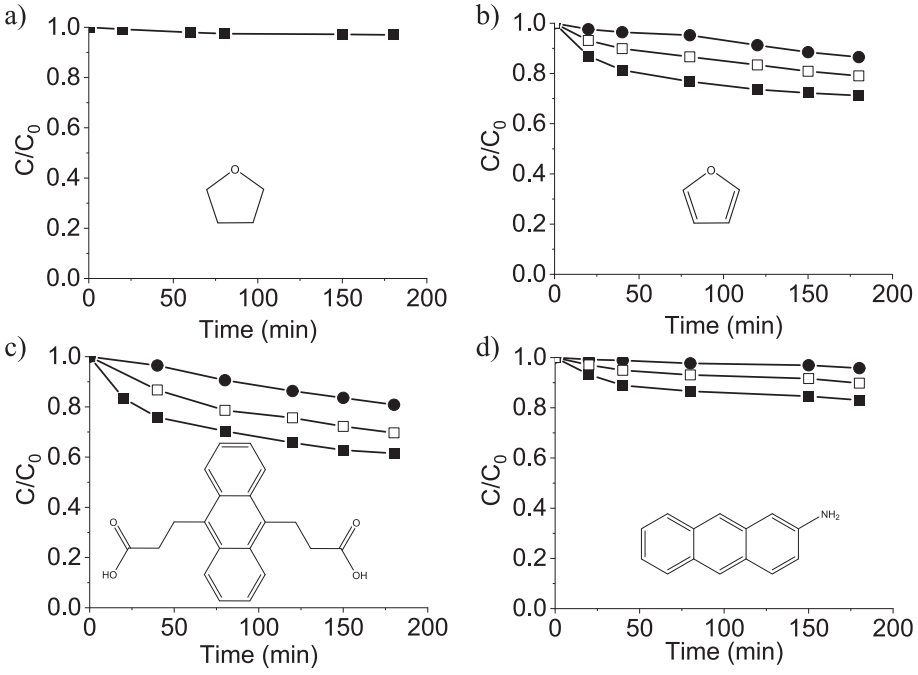

Fig. 7. Catalytic oxalic acid degradation by O_3 at pH 3 using a) tetrahydrofuran at 7.35 mM (■), b) furan at 7.35 mM (■), 2.94 mM (□) and 0.735 mM, c) 3,3′-(anthracene-9,10-diyl)dipropanoic acid at 7.35 mM (■), 2.94 mM (□) and 0.735 mM (●), and d) 2-aminoanthracene at 2.6 mM (■), 4.6 mM (□) and 6.7 mM (●). Reaction conditions: Oxalic acid (12.5 mg L^{-1}), pH 3, temperature 20 °C, O_3 inlet to the glass reactor (140 mg h^{-1}).

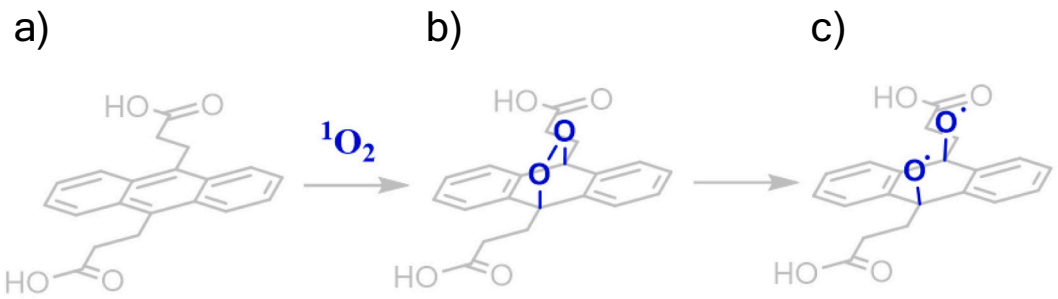

Scheme 2. Generation of bis oxyl radicals by $^1O_2$ formed from O_3 on a) 3,3′-(anthracene-9,10-diyl)dipropanoic acid as a model organocatalyst, b) 3,3′-(anthracene-9,10-diyl) endoperoxide dipropanoic acid and c) 3,3′-(anthracene-9,10-diyl) bis oxyl dipropanoic acid.

associated with the presence of endoperoxides. These facts might be due to the well-known unstable character of most organic peroxides [62] and, therefore, their decomposition during the required time to collect the sample and perform the FT-IR measurements (~ 2 min). Attempts to characterize the sample suspensions by Raman spectroscopy did not allow us to focus on the solid sample and record the spectrum. Attempts to dry the sample in a hot plate at 50 °C resulted in the absence of new Raman bands again associated with possible endoperoxide decomposition (Fig. S23 c,d).

3.4. Theoretical calculations

To lend some support to the experimental evidence about the formation of endoperoxides on the G, as precursor of peroxyl radical resulting in oxalic acid decomposition, computational calculations on graphitic carbon models were performed. Specifically, density functional theory (DFT) calculations were carried out to understand how the structural and steric features of α-G material modulate the reversible oxygen storage and subsequent activation for catalytic purposes. Previous experimental and theoretical related studies have reported the formation of aromatic endoperoxides within aromatic graphitic domains [63]. With these precedents, the formation of aromatic endoperoxide products by [4 + 2] cycloaddition of $^1O_2$ to different aromatic compounds [benzene (1), naphthalene (2), anthracene (3), phenanthrene (4) and pyrene (5)] was studied. The adsorption of $^1O_2$ on the top of these aromatic rings is favorable in all cases ranging from −3.8 (6) to −7.7 (3) kcal mol^{-1}. The obtained results indicate that additional fused rings decreased the activation barrier (ΔG, kcal mol^{-1}) in comparison to benzene as well as favouring the formation of the endoperoxides (Fig. 8a). However, this trend significantly changes for phenanthrene and pyrene. In those cases, the activation barriers are higher and the obtained endoperoxides are not thermodynamically favoured [$\Delta G_{product}$ = 1.4 (4) and 15.0 (5)]. Upon formation of these endoperoxides, they may follow two different dissociation pathways depending on the reaction conditions: (a) cycloreversion and (b) cleavage yielding more reactive bis oxyl radicals. Fig. 8a also shows the structure of a transition state in agreement to previous outcomes. In the transition state (TS) structures, the O═O length in its singlet state (RO=O = 1.19 Å) is increased up to 1.26–1.30 Å at PBE0-D3/def2-TZVP level. Like other cycloaddition reactions, [64,65] our activation barriers (ΔE‡) are dissected into distort$_i$on (ΔEd‡) and interaction (ΔEi‡) energies. To consider the steric strain of this cycloaddition, ΔEd‡ was selected since accounts for geometric and electronic changes to deform reactants into the transition state geometries. In particular, the electron reorganization (λ, also called π-relocalization energy) may correlate with the reactivity of these aromatic compounds, this term being also included within the distortion energies. However, our DFT calculations suggest different points: (i) ΔEd‡ considering exclusively the distortion of the aromatic ring controls the calculated ΔG‡ (R^2 = 0.927); (ii) Electron reorganization does not properly account the observed trend for ΔG‡ or ΔG_{rxn}. In that case, benzene and pyrene failed in the correlation.

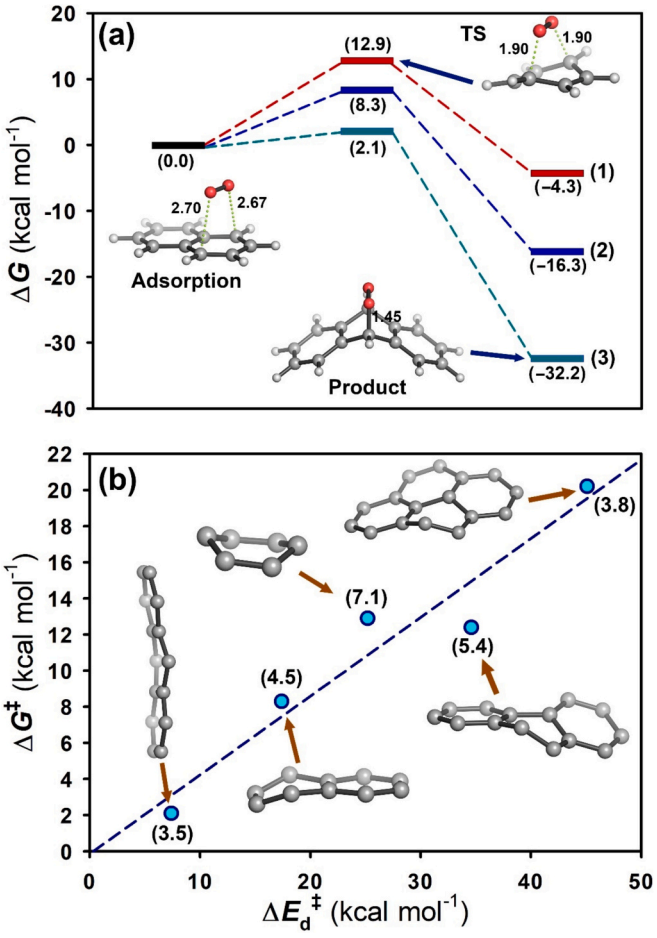

Fig. 8. a) Reaction coordinate for the [4 + 2] cycloaddition to benzene (1, in red), naphthalene (2, in blue) and anthracene (3, in green); b) Plot of PBE0-D3/def2-TZVP distortion energies versus free energy of the activation barriers. The electron reorganization energies (in kcal mol^{-1}) are shown in parenthesis. Distances are given in Å.

DFT calculations were also performed to predict the capability of anthracene endoperoxide model compound to form bis oxyl radicals and their ability to degrade oxalic acid (Fig. S24). The calculated energy barrier for the formation of oxyl biradicals from anthracene endoperoxide is 22.5 kcal mol^{-1}, which agrees with our experimental results, as this barrier can be overcome at our working temperature. In this profile, we considered both singlet and triplet states based on previous studies. [66] The calculated O—O bond dissociation energy and oxyl radical formation via thermolysis energy is 21.5 kcal mol^{-1}, which is consistent with common endoperoxide values reported in the literature. [58] Subsequently, these oxyl radicals can rearrange to yield a bis epoxide

and its isomerized form. Both species are more stable (−40.8 and − 42.7 kcal mol^{-1}, respectively) than the oxyl biradical.

To evaluate the ability anthracene endoperoxide model to oxidize oxalic acid under these conditions, we identified as most plausible oxidation site in the α-G model a ketone / hydroxy pair as a representative structure to oxidize oxalic acid (at pH = 3). Then, we predicted the reduction potential of our anthracene endoperoxide system (E^0 versus SHE = −0.45 V). Based on these species, oxyl biradicals can be reduced by oxalic acid [$E^0(CO_2/H_2C_2O_4)$ = −0.475 V versus SHE] as illustrated in Fig. S24. [67]

These considerations were employed as initial findings to understand the formation of endoperoxides in tube models of G microporous channels. It should be noted that channel structure in G materials is shown in Fig. 9 and these data are provided from the previous HR-TEM (Figs. 2 and S5) and isothermal N_2 sorption measurements (Fig. S6). Two feasible adsorption modes were considered as well as three pore sizes (0.36, 0.48 and 0.57 nm) (Fig. 9a). Firstly, the adsorption is not possible for the material with smaller pore size (0.36 nm) whereas on the surface the adsorption energy was −8.4 kcal mol^{-1}. For a higher pore size (0.48 nm), an ΔE_{ads} of 29.5 kcal mol^{-1} inside the tube shows that this process is not favoured (Fig. 9b). On the contrary, the adsorption of $^1O_2$ on the surface proved to be feasible (ΔE_{ads} = −7.5 kcal mol^{-1}). Increasing the pore size has a dramatic impact on the adsorption inside the carbon tube. For a pore size of 0.57 nm, the calculated ΔE_{ads} indicates that under these conditions both adsorption modes are equally favoured (−9.5 and − 8.4 for the surface and inside the tube, respectively).

After adsorption, both pore sizes (0.48 and 0.57 nm) exhibit endothermic endoperoxide adducts with ΔE values of 10.6 and 16.6 kcal mol^{-1} thus suggesting that this process is not favorable at least at room temperature. These adducts display a O—O bond length larger than $^1O_2$ ($\Delta R_{O\text{-}O}$ = 0.29 Å) thus indicating that these species are activated for catalytic purposes. Another situation was found for the model of the smallest pore size (0.36 nm). This system is extremely constrained and ends up relaxed upon endoperoxide formation (ΔE = −13.7 kcal mol^{-1}). Thus, these calculations indicate that endoperoxide formation should be favoured for G materials with smaller pore size, such as α-G.

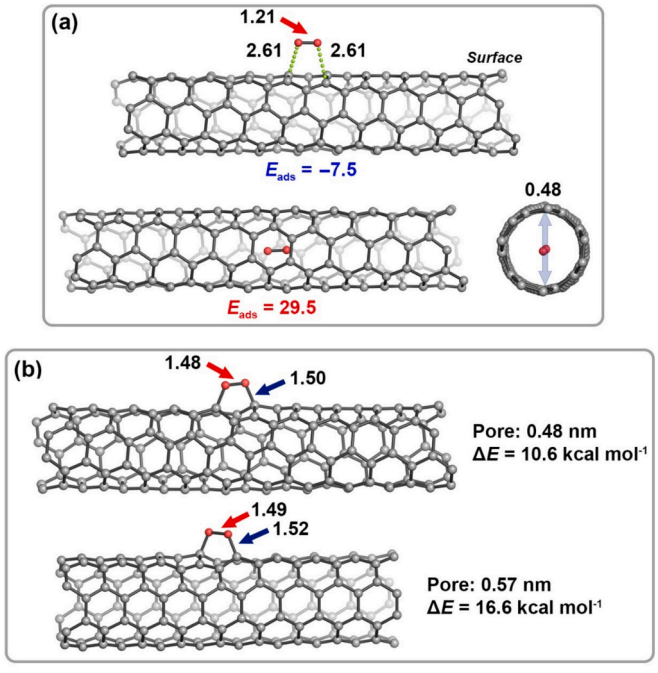

Fig. 9. a) Adsorption process of $^1O_2$ on the surface of a carbon tube model (0.48 nm) as well as inside the material; b) Formation of endoperoxide adducts at two pore size (0.48 and 0.57 nm). Energies are given in kcal mol^{-1} and distances in Å.

It is known that curvature of these kinds of systems affects the chemical reactivity. Different parameters have been described to account this relationship, for example, the pyramidalization angle (θ_p) [66,67]. From this parameter, $\theta_p = 0^\circ$ corresponds to a planar system (sp^2-hybridized carbon atom) whereas $\theta_p = 19.5^\circ$ for a sp^3-hybridized atom. For this angle, large values correlate with higher reactivity. In our model, we have applied an estimation from the $\Delta E_d^{\ddagger}$ obtained for small aromatic rings. Curved π-extended carbon tubes are structurally strained thus minimizing the distortion penalty of activation barriers. Therefore, both endoperoxide and di oxyl formation should be favorable in the convex face of the tube or channels, while $^1O_2$ activation inside the carbon species should be unfavorable due to large $\Delta E_d^{\ddagger}$ values.

As indicated by theoretical modelling, pore size influences in two different ways. When the pore size is smaller than the kinetic diameter of O_3 and $^1O_2$ the reaction occurs on the external surface since the internal diffusion does not occur. In addition, due to the smaller diameter of the curvature of the graphitic walls is larger, and this geometrical strain favors the reactivity with $^1O_2$ and formation of the endoperoxide. In other words, curved surfaces are more reactive than when the surface is flat. Overall, experimental and theoretical evidence confirm the feasibility of as-prepared α-, β- and γ-Gs derived carbons efficiently promote $^1O_2$ activation through endoperoxide dependent on the pore dimensions.

4. Conclusions

This work has demonstrated the activity of cyclodextrin-derived graphitic carbons as metal-free ozonation catalysts for oxalic acid degradation in water. The observed order of activity was α-G followed by β-G and γ-G. The activity of α-G corresponds to the material with less defective graphitic structure and the highest surface area that corresponds to extended aromatic electron rich domains as evidenced by spectroscopic and analytical characterization. Importantly, α-G is a catalyst that achieved full oxalic acid degradation in a wide range of pH values from 3 to 11. Furthermore, the use of only 50 mg L^{-1} α-G can degrade 1 g L^{-1} of oxalic acid. This performance compares favorably with previous analogous reports using other biomass derived carbocatalysts or activated carbons while there is still room for improvement to achieve the record activities of other synthetic carbons such as nanographite. [30,37,43] We attribute this improved catalytic activity as an effect of microporosity. It was found that α-G gradually deactivates upon reuse due to its partial oxidation, but its initial activity can be recovered completely by pyrolysis. Importantly, it was found that the mechanism using microporous Gs involves the capture of $^1O_2$ by the polycyclic aromatic domains of the carbocatalyst, probably resulting in endoperoxide like intermediates that activate oxalic acid through oxyl radicals derived from endoperoxide ring opening. Thus, no direct contact between O_3 and oxalic acid is necessary in the α-G promoted decomposition. The consumption of these domains, which are susceptible to the $O_3/^1O_2$ attack, results in a gradual deactivation of the carbocatalyst and a simultaneous increase in oxygen content. This deactivation process can be reversed by thermal treatment, which is known to remove small oxygenated species from carbons, increasing the graphitization degree. This understanding of the process has allowed us to explore the catalytic activity of simple organic molecules as sacrificial agents, bridging the gap between carbocatalysis and organocatalysis. The present results challenge the current use of oxalic acid as the chosen sacrificial molecule for selective electron transfer decomposition promoted by O_3 and highlights the role that $^1O_2$ can play in O_3-promoted decomposition also supported by DFT calculations. Unlike most related precedents, this investigation has found novel findings about the importance of $^1O_2$ during ozonation by metal-free catalysts via non-radical mediated oxalic acid degradation.

CRediT authorship contribution statement

Antón López-Francés: Investigation. **Ana García-Mulero:** Investigation. **Emanuela Accardo:** Software, Investigation. **Belén Ferrer:** Formal analysis. **Antonio Franconetti:** Investigation. **Ana Primo:** Project administration. **Amarajothi Dhakshinamoorthy:** Writing – review & editing, Writing – original draft, Supervision, Project administration. **Sergio Navalón:** Writing – review & editing, Writing – original draft, Funding acquisition, Conceptualization. **Hermenegildo García:** Writing – review & editing, Project administration.

Declaration of competing interest

The authors declare that they have no known competing financial interests or personal relationships that could have appeared to influence the work reported in this paper.

Acknowledgements

A.D. is beneficiary of a grant María Zambrano in Universitat Politècnica de València within the framework of the grants for the retraining in the Spanish university system (Spanish Ministry of Universities, financed by the European Union, NextGeneration EU). The center of Supercomputing of Galicia (CESGA) for the computational facilities is acknowledged. S.N. thanks the support received from Grant PID2021–123856OB-I00 funded by MICIU/AEI/10.13039/501100011033 and by ERDF A way of making Europe. Funding for open access charge: CRUE-Universitat Politècnica de València.

Appendix A. Supplementary data

Supplementary data to this article can be found online at https://doi.org/10.1016/j.cej.2025.166971.

Data availability

Data will be made available on request.

References

[1] V.I. Parvulescu, F. Epron, H. Garcia, P. Granger, Recent progress and prospects in catalytic water treatment, Chem. Rev. 122 (2022) 2981–3121, https://doi.org/10.1021/acs.chemrev.1c00527.
[2] Y. Shang, X. Xu, B. Gao, S. Wang, X. Duan, Single-atom catalysis in advanced oxidation processes for environmental remediation, Chem. Soc. Rev. 50 (2021) 5281–5322, https://doi.org/10.1039/D0CS01032D.
[3] P. Hu, M. Long, Cobalt-catalyzed sulfate radical-based advanced oxidation: a review on heterogeneous catalysts and applications, Appl. Catal. B 181 (2016) 103–117, https://doi.org/10.1016/j.apcatb.2015.07.024.
[4] J.J. Pignatello, E. Oliveros, A. MacKay, Advanced oxidation processes for organic contaminant destruction based on the Fenton reaction and related chemistry, Crit. Rev. Environ. Sci. Technol. 36 (2006) 1–84, https://doi.org/10.1080/10643380500326564.
[5] B. Kasprzyk-Hordern, M. Ziółek, J. Nawrocki, Catalytic ozonation and methods of enhancing molecular ozone reactions in water treatment, Appl. Catal. Environ. 46 (2003) 639–669, https://doi.org/10.1016/S0926-3373(03)00326-6.
[6] J. Nawrocki, B. Kasprzyk-Hordern, The efficiency and mechanisms of catalytic ozonation, Appl Catal B 99 (2010) 27–42, https://doi.org/10.1016/j.apcatb.2010.06.033.
[7] C.V. Rekhate, J.K. Srivastava, Recent advances in ozone-based advanced oxidation processes for treatment of wastewater- a review, Chem. Eng. J. Adv. 3 (2020) 100031, https://doi.org/10.1016/j.ceja.2020.100031.
[8] Y. Wang, G. Yu, Challenges and pitfalls in the investigation of the catalytic ozonation mechanism: a critical review, J. Hazard. Mater. 436 (2022) 129157, https://doi.org/10.1016/j.jhazmat.2022.129157.
[9] S. Navalon, A. Dhakshinamoorthy, M. Alvaro, H. Garcia, Heterogeneous Fenton catalysts based on activated carbon and related materials, ChemSusChem 4 (2011) 1712–1730, https://doi.org/10.1002/cssc.201100216.
[10] M. Kohantorabi, G. Moussavi, S. Giannakis, A review of the innovations in metal- and carbon-based catalysts explored for heterogeneous peroxymonosulfate (PMS) activation, with focus on radical vs. non-radical degradation pathways of organic contaminants, Chem. Eng. J. 411 (2021) 127957, https://doi.org/10.1016/j.cej.2020.127957.
[11] W.D. Oh, Z. Dong, T.T. Lim, Generation of sulfate radical through heterogeneous catalysis for organic contaminants removal: current development, challenges and prospects, Appl Catal B 194 (2016) 169–201, https://doi.org/10.1016/j.apcatb.2016.04.003.
[12] H. Luo, H. Fu, H. Yin, Q. Lin, Carbon materials in persulfate-based advanced oxidation processes: the roles and construction of active sites, J. Hazard. Mater. (2022) 128044, https://doi.org/10.1016/j.jhazmat.2021.128044.
[13] J. Wang, H. Chen, Catalytic ozonation for water and wastewater treatment: recent advances and perspective, Sci. Total Environ. 704 (2020) 135249, https://doi.org/10.1016/j.scitotenv.2019.135249.
[14] U. Von Gunten, Ozonation of drinking water: part I. oxidation kinetics and product formation, Water Res. 37 (2003) 1443–1467, https://doi.org/10.1016/S0043-1354(02)00457-8.
[15] D.S. Su, S. Perathoner, G. Centi, Nanocarbons for the development of advanced catalysts, Chem. Rev. 113 (2013) 5782–5816, https://doi.org/10.1021/cr300367d.
[16] D.S. Su, G. Wen, S. Wu, F. Peng, R. Schlögl, Carbocatalysis in liquid-phase reactions, Angew. Chem. Int. Ed. 56 (2017) 936–964, https://doi.org/10.1002/anie.201600906.
[17] Y. Zhai, Z. Zhu, S. Dong, Carbon-based nanostructures for advanced catalysis, ChemCatChem 7 (2015) 2806–2815, https://doi.org/10.1002/cctc.201500323.
[18] Y. Liu, C. Chen, X. Duan, S. Wang, Y. Wang, Carbocatalytic ozonation toward advanced water purification, J Mater Chem A 9 (2019) 18994–19024, https://doi.org/10.1039/D1TA02953C.
[19] Y. Wang, X. Duan, Y. Xie, H. Sun, S. Wang, Nanocarbon-based catalytic ozonation for aqueous oxidation: engineering defects for active sites and tunable reaction pathways, ACS Catal. (22) (2020) 13383–13414, https://doi.org/10.1021/acscatal.0c04232.
[20] B. Daelemans, N. Bilbao, W. Dehaen, S. De Feyter, Carbocatalysis with pristine graphite: on-surface nanochemistry assists solution-based catalysis, Chem. Soc. Rev. 50 (2021) 2280–2296, https://doi.org/10.1039/D0CS01294G.
[21] S. Navalón, W.J. Ong, X. Duan, Sustainable catalytic processes driven by graphene-based materials, Processes 8 (2020) 672, https://doi.org/10.3390/pr8060672.
[22] S. Navalón, J.R. Herance, M. Álvaro, H. García, General aspects in the use of graphenes in catalysis, Mater. Horiz. 5 (2018) 363–378, https://doi.org/10.1039/C8MH00066B.
[23] L. Wu, T. Wu, Z. Liu, W. Tang, S. Xiao, B. Shao, Q. Liang, Q. He, Y. Pan, Y. Liu, S. Tong, Carbon nanotube-based materials for persulfate activation to degrade organic contaminants: properties, mechanisms and modification insights, J. Hazard. Mater. 431 (2022) 128536, https://doi.org/10.1016/j.jhazmat.2022.128536.
[24] S. Navalón, A. Dhakshinamoorthy, M. Álvaro, H. García, Diamond nanoparticles in heterogeneous catalysis, Chem. Mater. 32 (2020) 4116–4143, https://doi.org/10.1021/acs.chemmater.0c00204.
[25] S. Navalon, A. Dhakshinamoorthy, M. Alvaro, M. Antonietti, H. García, Active sites on graphene-based materials as metal-free catalysts, Chem. Soc. Rev. 46 (2017) 4501–4529, https://doi.org/10.1039/C7CS00156H.
[26] T. Jiang, B. Wang, B. Gao, N. Cheng, Q. Feng, M. Chen, S. Wang, Degradation of organic pollutants from water by biochar-assisted advanced oxidation processes: mechanisms and applications, J. Hazard. Mater. 442 (2023) 130075, https://doi.org/10.1016/j.jhazmat.2022.130075.
[27] A.A. Stepacheva, M.E. Markova, Y.V. Lugovoy, Y.Y. Kosivtsov, V.G. Matveeva, M. G. Sulman, Plant-biomass-derived carbon materials as catalyst support, a brief review, Catalysts 13 (2023) 655, https://doi.org/10.3390/catal13040655.
[28] A. Ahmad, M. Priyadarshini, S. Yadav, M.M. Ghangrekar, R.Y. Surampalli, The potential of biochar-based catalysts in advanced treatment technologies for efficacious removal of persistent organic pollutants from wastewater: a review, Chem. Eng. Res. Des. 187 (2022) 470–496, https://doi.org/10.1016/j.cherd.2022.09.024.
[29] A. Rendón-Patiño, A. Santiago-Portillo, C. Vallés-Garcia, M. Palomino, S. Navalón, A. Franconetti, A. Primo, H. Garcia, Templateless synthesis of ultra-microporous 3D graphitic carbon from cyclodextrins and their use as selective catalyst for oxygen activation, Small Methods 4 (2020) 1900721, https://doi.org/10.1002/smtd.201900721.
[30] A. López-Francés, M. Cabrero-Antonino, F. Bernat-Quesada, B. Ferrer, M. Blanes, R. García, P. Almenar, M. Álvaro, A. Dhakshinamoorthy, H.G. Baldoví, S. Navalón, Valorization of field-spent granular activated carbon as heterogeneous ozonation catalyst for water treatment, ChemSusChem (2024) e202400062, https://doi.org/10.1002/cssc.202400062.
[31] F. Bernat-Quesada, J.C. Espinosa, V. Barbera, M. Álvaro, M. Galimberti, S. Navalon, H. García, Catalytic ozonation using edge-hydroxylated graphite-based baterials, ACS Sustain. Chem. Eng. 7 (2019) 17443–17452, https://doi.org/10.1021/acssuschemeng.9b04646.
[32] A. López-Francés, F. Bernat-Quesada, M. Cabrero-Antonino, B. Ferrer, A. Dhakshinamoorthy, H.G. Baldoví, S. Navalón, Nanographite: a highly active and durable metal-free ozonation catalyst with application in natural waters, Appl. Catal. B.-Environ. 336 (2023) 122924, https://doi.org/10.1016/j.apcatb.2023.122924.
[33] Y. Song, S. Feng, W. Qin, J. Ma, Mechanism of catalytic ozonation in expanded graphite aqueous suspension for the degradation of organic acids, Environ. Technol. (2021) 739–750, https://doi.org/10.1080/09593330.2021.1983024.
[34] M. Wang, Z. Wang, Y. Wang, R. Li, Y. Zhang, C. Liu, Y. Liu, B. Xu, F. Qi, Insights into heteroatom-doped graphene for catalytic ozonation: active centers, reactive oxygen species evolution, and catalytic mechanism, Environ. Sci. Technol. 53 (2019) 5337–5348, https://doi.org/10.1021/acs.est.9b01361.

[35] Y. Wang, Y. Xie, H. Sun, J. Xiao, H. Cao, S. Wang, Efficient catalytic ozonation over reduced graphene oxide for p-hydroxylbenzoic acid (PHBA) destruction: active site and mechanism, ACS Appl. Mater. Interfaces 8 (2016) 9710–9720, https://doi.org/10.1021/acsami.6b01175.
[36] F. Bernat-Quesada, C. Vallés-García, E. Montero-Lanzuela, A. López-Francés, B. Ferrer, H.G.G. Baldoví, S. Navalón, Hybrid sp2/sp3 nanodiamonds as heterogeneous metal-free ozonation catalysts in water, Appl. Catal. B Environ. 299 (2021) 120673, https://doi.org/10.1016/j.apcatb.2021.120673.
[37] A. López-Francés, L. Peng, F. Bernat-Quesada, B. Ferrer, S. Navalón, A. Dhakshinamoorthy, H. García, Biopolymer-derived structured graphitic carbons as metal-free heterogeneous ozonation catalysts in water, Mater Today Sustain 27 (2024) 100807, https://doi.org/10.1016/j.mtsust.2024.100807.
[38] I.K.M. Yu, X. Xiong, D.C.W. Tsang, Y.H. Ng, J.H. Clark, J. Fan, S. Zhang, C. Hu, Y. S. Ok, Graphite oxide- and graphene oxide-supported catalysts for microwaveassisted glucose isomerisation in water, Green Chem. 21 (2019) 4341–4353, https://doi.org/10.1039/C9GC00734B.
[39] J. Zhou, J. Jia, J. He, J. Li, J. Cai, Cyclodextrin inclusion complexes and their application in food safety analysis: recent developments and future prospects, Foods 30 (2022) 3871, https://doi.org/10.3390/foods11233871.
[40] M.P. Di Cagno, The potential of cyclodextrins as novel active pharmaceutical ingredients: a short overview, Molecules 22 (2017) 1, https://doi.org/10.3390/molecules22010001.
[41] J.L. Figueiredo, M.F.R. Pereira, The role of surface chemistry in catalysis with carbons, Catal. Today 150 (2010) 2–7, https://doi.org/10.1016/j.cattod.2009.04.010.
[42] J. Yang, Z. Zhang, J. Wang, X. Zhao, Y. Zhao, J. Qian, T. Wang, Pyrolysis and hydrothermal carbonization of biowaste: a comparative review on the conversion pathways and potential applications of char product, Sustain. Chem. Pharm. 33 (2023) 101106, https://doi.org/10.1016/j.scp.2023.101106.
[43] A. López-Francés, B. Ferrer, H.G. Baldoví, A. Dhakshinamoorthy, S. Navalón, Engineering of activated biochar derived from pine needle waste biomass as ozonation catalyst in water, Adv. Sust. Syst. (2025) 2500108, https://doi.org/10.1002/adsu.202500108.
[44] J. Wang, S. Chen, X. Quan, H. Yu, Fluorine-doped carbon nanotubes as an efficient metal-free catalyst for destruction of organic pollutants in catalytic ozonation, Chemosphere 190 (2018) 135–143, https://doi.org/10.1016/j.chemosphere.2017.09.119.
[45] F.J. Beltrán, F.J. Rivas, F.A. Fernánndez, P.M. Álvarez, R. Montero-de-Espinosa, Kinetics of catalytic ozonation of oxalic acid in water with activated carbon, Ind. Eng. Chem. Res. 41 (2002) 6510–6517, https://doi.org/10.1021/ie020311d.
[46] S. Canonica, T. Kohn, M. Mac, F.J. Real, J. Wirz, U. von Gunten, Photosensitizer method to determine rate constants for the reaction of carbonate radical with organic compounds, Environ. Sci. Technol. 39 (2005) 9182–9188, https://doi.org/10.1021/es051236b.
[47] Q. Yang, Y. Ma, F. Chen, F. Yao, J. Sun, S. Wang, K. Yi, L. Hou, X. Li, D. Wang, Recent advances in photoactivated sulfate radical-advanced oxidation process (SR-AOP) for refractory organic pollutants removal in water, Chem. Eng. J. 378 (2019) e122149, https://doi.org/10.1016/j.cej.2019.122149.
[48] W. Yang, T. Wu, Investigation of matrix effects in laboratory studies of catalytic ozonation processes, Ind. Eng. Chem. Res. 58 (2019) 3468–3477, https://doi.org/10.1021/acs.iecr.8b05465.
[49] L. Wang, K. Xiao, H. Zhao, The debatable role of singlet oxygen in persulfate-based advanced oxidation processes, Water Res. 235 (2023) 119925, https://doi.org/10.1016/j.watres.2023.119925.
[50] P.C.C. Faria, J.J.M. Órfão, M.F.R. Pereira, Activated carbon catalytic ozonation of oxamic and oxalic acids, Appl. Catal. B Environ. 79 (2008) 237–243, https://doi.org/10.1016/j.apcatb.2007.10.021.
[51] Z.Q. Liu, J. Ma, Y.-H. Cui, B.-P. Zhang, Effect of ozonation pretreatment on the surface properties and catalytic activity of multi-walled carbon nanotube, Appl. Catal. B Environ. 92 (2009) 301–306, https://doi.org/10.1016/j.apcatb.2009.08.007.
[52] S. Zhang, X. Quan, J.F. Zheng, D. Wang, Probing the interphase 'HO* zone' originated by carbon nanotube during catalytic ozonation, Water Res. 122 (2017) 86–95, https://doi.org/10.1016/j.watres.2017.05.063.
[53] G.R. Buettner, Spin trapping: ESR parameters of spin adducts 1474 1528V, Free Radic. Biol. Med. 3 (4) (1987) 259–303, https://doi.org/10.1016/S0891-5849(87)80033-3.
[54] Y. Guo, E. Zhao, J. Long, G. Yu, Y. Wang, Quantification of the contribution of heterogeneous surface processes to pollutant abatement during heterogeneous catalytic ozonation, Environ. Sci. Technol. 58 (2024) 18992–19003, https://doi.org/10.1021/acs.est.4c06804.
[55] Z. Barbieriková, M. Mihalíková, V. Brezová, Photoinduced oxidation of sterically hindered amines in acetonitrile solutions and titania suspensions (an EPR study), Photochem. Photobiol. 88 (2012) 1442–1454, https://doi.org/10.1111/j.1751-1097.2012.01189.x.
[56] J.C. Espinosa, M. Álvaro, A. Dhakshinamoorthy, S. Navalón, H. García, Engineering active sites in reduced graphene oxide: tuning the catalytic activity for aerobic oxidation, ACS Sustain. Chem. Eng. 7 (19) (2019) 15948–15956, https://doi.org/10.1021/acssuschemeng.9b02237.
[57] J.C. Espinosa, S. Navalon, M. Alvaro, A. Dhakshinamoorthy, H. Garcia, Reduction of C=C double bonds by hydrazine using active carbons as metal-free catalysts, ACS Sustain. Chem. Eng. 6 (2018) 5607–5614, https://doi.org/10.1021/acssuschemeng.8b00638.
[58] E.L. Clennan, Aromatic endoperoxides, Photochem. Photobiol. 99 (2023) 204–220, https://doi.org/10.1111/php.13674.
[59] H. Fidder, A. Lauer, W. Freyer, B. Koeppe, K. Heyne, Photochemistry of anthracene-9,10-endoperoxide, J. Phys. Chem. A 113 (2009) 6289–6296, https://doi.org/10.1021/jp901073s.
[60] V. Fabregat, M.I. Burguete, F. Galindo, S.V. Luis, Singlet oxygen generation by photoactive polymeric microparticles with enhanced aqueous compatibility, Environ. Sci. Pollut. Res. 21 (2014) 11884–11892, https://doi.org/10.1007/s11356-013-2311-8.
[61] P. Di Mascio, E.J.H. Bechara, J.C. Rubim, Dioxygen NIR FT-emission ($1\Delta g \rightarrow 3\Sigma$-g) and Raman spectra of 1, 4-dimethylnaphthalene endoperoxide: a source of singlet molecular oxygen, Appl. Spectrosc. 46 (1992) 236–239, https://doi.org/10.1366/000370292412.
[62] V. Vacque, B. Sombret, J.P. Huvenne, P. Legrand, S. Suc, Characterisation of the O–O peroxide bond by vibrational spectroscopy, Spectrochimica Acta Part A: Molecular and Biomolecular Spectroscopy 53 (1997) 55–66, https://doi.org/10.1016/S1386-1425(97)83009-0.
[63] J.M. Aubry, C. Pierlot, J. Rigaudy, R. Schmidt, Reversible binding of oxygen to aromatic compounds, Acc. Chem. Res. 36 (2003) 668–675, https://doi.org/10.1021/ar010086g.
[64] D.H. Ess, K.N. Houk, Distortion/interaction energy control of 1,3-dipolar cycloaddition reactivity, J. Am. Chem. Soc. 29 (2007) 10646–10647, https://doi.org/10.1021/ja0734086.
[65] D.H. Ess, Distortion, interaction, and conceptual DFT perspectives of MO 4-alkene (M = Os, Re, Tc, Mn) cycloadditions, J. Org. Chem. 74 (2009) 1498–1508, https://doi.org/10.1021/jo802189w.
[66] S. Park, D. Srivastava, K. Cho, Generalized chemical reactivity of curved surfaces: carbon nanotubes, Nano Lett. 3 (2003) 1273–1277, https://doi.org/10.1021/nl0342747.
[67] T. Lin, W.-D. Zhang, J. Huang, C. He, A DFT study of the amination of fullerenes and carbon nanotubes: reactivity and curvature, J. Phys. Chem. C 109 (2005) 13755–13760, https://doi.org/10.1021/jp051022g.